

Localization Exploiting Spatial Variations in the Magnetic Field: Principles and Challenges

Isaac Skog, *Senior Member, IEEE*, Manon Kok, *Member, IEEE*, Christophe Prieur, *Fellow, IEEE*, and Gustaf Hendeby, *Senior Member, IEEE*

arXiv:2602.14181v1 [eess.SP] 15 Feb 2026

SIGNAL processing has played, and continues to play, a fundamental role in the evolution of modern localization technologies. Localization using spatial variations in the Earth's magnetic field is no exception. It relies on signal-processing methods for statistical state inference, magnetic-field modeling, and sensor calibration. Contemporary localization techniques based upon spatial variations in the magnetic field can provide decimeter-level localization accuracy indoors [1], and outdoor localization accuracy on par with strategic-grade inertial navigation systems [2]. This article provides a broad, high-level overview of current signal-processing principles and open research challenges in localization using spatial variations in the Earth's magnetic field. The aim is to provide the reader with an understanding of the similarities and differences among existing key technologies from a statistical signal-processing perspective. To that end, existing key technologies will be presented within a common parametric signal-model framework compatible with well-established statistical inference methods. A comprehensive treatment of all types of magnetic-field-based localization technologies is beyond the scope of this article; interested readers are referred to the survey articles [3–6], which have different focuses. Specifically, [3] describes existing techniques for magnetic-field indoor localization, and challenges related to large-scale use of these techniques, [4] provides a high-level system description of magnetic-field localization, including the generation of artificial magnetic fields, [5] focuses on robotics applications, and [6] focuses on smartphone-based indoor localization.

The use of the Earth's magnetic field for localization and navigation dates back over a millennium to the introduction of the first compasses. However, it was not until about half a century ago that research on the use of spatial variations in the Earth's magnetic field for localization began [7]. The main application areas were then aerospace and marine systems. With the introduction of miniaturized electronic magnetometers in the early 2000s and their subsequent integration into smartphones, the field of indoor localization for robots and humans using magnetic-field variations flourished. Here, the signal processing community has played and continues to

play a crucial role by providing theoretically sound and efficient principles for modeling sensor measurements [8] and the spatial variation in the magnetic field [9], as well as performing statistical inference to infer the parameters of these models [10].

Recently, driven by geopolitical concerns about jamming and spoofing of global navigation satellite systems (GNSSs) and other radio-based localization technologies, there has been renewed interest in magnetic-field localization techniques for classical aerospace and marine systems, as well as various emerging autonomous systems. Magnetic field-based localization possesses the properties of being passive and thereby stealthy, and challenging to jam on a large scale since the field strength decays cubically with distance. This renewed interest in using magnetic field-based localization techniques as a complement to GNSSs-based localization, along with the emergence of affordable, power-efficient, and compact high-performance magnetometers based on quantum sensing technology, has created new research challenges and opportunities.

The outline of the article is as follows. First, key technologies for localization based on spatial variations in the magnetic field are introduced from a Bayesian perspective. Subsequently, mathematical models of magnetic fields and magnetometers are introduced and used to define a parametric signal model framework. Thereafter, statistical inference for magnetic-field map learning and localization using the parametric signal model framework is discussed. The article concludes with a discussion on open research challenges and a technology outlook.

INTRODUCTION

Although the Earth's magnetic field is commonly approximated as a constant dipole field, local spatial variations in the ambient magnetic field are omnipresent. The spatial variations are caused by ferromagnetic materials in the Earth's lithosphere and by man-made structures, which interact with the magnetic field generated by the Earth's core [7]. Two examples of these field variations, indoor and outdoor, are shown in Fig. 1. Although the figure illustrates the spatial variations in field magnitude, it is worth emphasizing that the magnetic field is a three-component vector field, and these spatial variations occur in all three components; see Fig. 1a. Moreover, the field is also temporally varying due to magnetospheric disturbances, solar storms, etc.; see Fig. 1b. These temporal variations are typically on the order of tens to hundreds of nano-Tesla. For indoor localizations, where the spatial variations are on the

I. Skog is with the KTH Royal Institute of Technology, Sweden, FOI Swedish Defence Research Agency, and Digital Futures. email: skog@kth.se
M. Kok is with the Delft University of Technology, the Netherlands. email: m.kok-1@tudelft.nl

C. Prieur is with the University Grenoble Alpes, CNRS, Grenoble-INP, GIPSA-Lab, F-38000 Grenoble, France. email: christophe.prieur@gipsa-lab.fr

G. Hendeby is with Linköping University, Sweden. email: gustaf.hendeby@liu.se

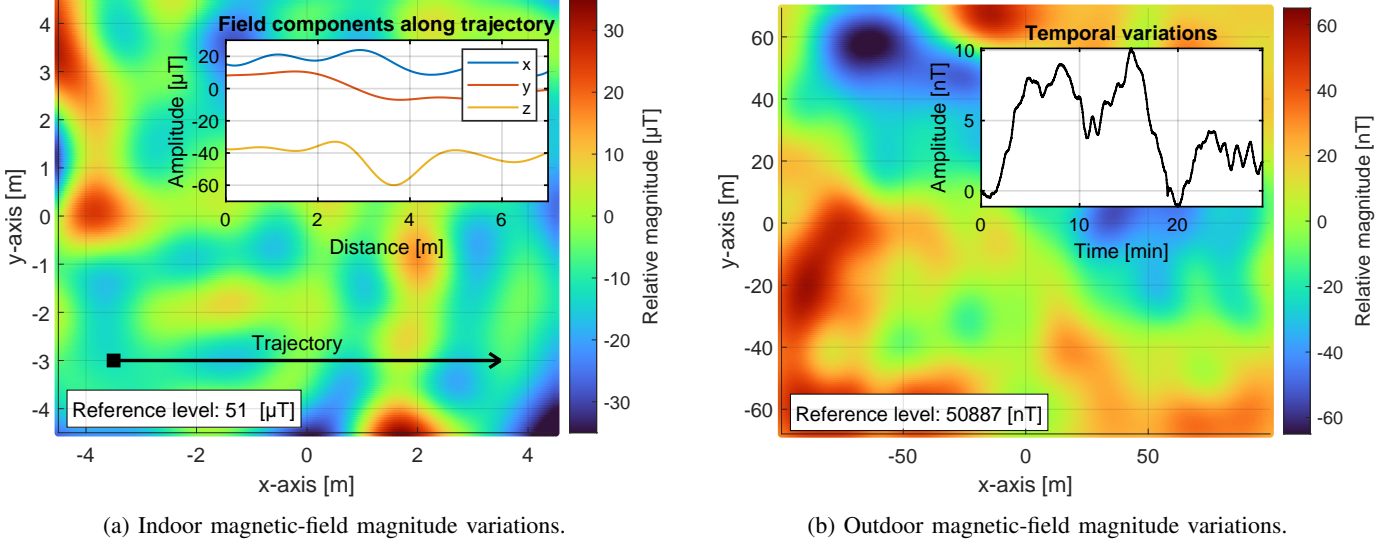


Fig. 1: Examples of the spatial variations in the magnetic field-magnitude indoors and outdoors. Also shown in (a) are the three field components along the trajectory indicated by the black arrow. Also shown in (b) is an example of temporal variations in the magnetic field during 30 minutes. Note the significant difference in length and magnitude scale indoors and outdoors.

order of tens of micro-Tesla, they are typically neglected. In outdoor localization, where spatial variations are on the order of tens to hundreds of nano-Tesla, they may be compensated for using data from a stationary reference magnetometer. Since this article focuses on localization using spatial variations in the magnetic field, temporal variations are disregarded unless explicitly stated otherwise, and all fields are assumed static.

Localization techniques

Localization refers to the process of inferring the state x_t of a localization system at time instant t from measurements. The state x_t at least includes the location r_t , but is frequently augmented with quantities such as the orientation q_t and velocity v_t , required to describe the sensor measurements and the motion of the platform carrying the localization system. There are three main techniques for localization exploiting spatial variations in the Earth's magnetic field \mathcal{B} : map matching, simultaneous localization and mapping (SLAM), and dead-reckoning.

Magnetic-field map matching, where the state x_t is inferred by matching a sequence of magnetometer measurements $y_{1:t}$ to a map \mathcal{M} . The map, directly or indirectly, describes the magnetic field \mathcal{B} , the magnitude $\|\mathcal{B}\|$, or the field potential as a function of the location r_t . If the features within the map \mathcal{M} are linked to a global frame of reference, this technique provides absolute location with a bounded location error.

Magnetic-field SLAM, where the magnetometer measurements $y_{1:t}$ are simultaneously used to construct a map \mathcal{M} and infer the state x_t with respect to this map. Without additional measurements linked to a global frame of reference, this technique only provides relative location with respect to the initial system state x_0 . When new areas are mapped, the location error grows unboundedly, whereas revisiting already mapped areas keeps the error bounded.

Magnetic-field dead reckoning, where translation and orientation information is extracted from the magnetic field using a time-varying local map, and accumulated to infer the state x_t relative to an initial pose x_0 . This can be viewed as a degenerate form of magnetic-field SLAM, in which the map \mathcal{M} is purely local and not retained over time. As for all dead-reckoning techniques, the location error grows without bound. Notably, for magnetic field dead-reckoning to function in practice, measurements from an array of magnetometers are required.

The map \mathcal{M} used in these three localization techniques may be deterministic or stochastic. In the stochastic case, it is characterized by a probability density $p(\mathcal{M})$ and can capture uncertainties about the map. In the subsequent discussion, the map is assumed to be stochastic, with the deterministic case regarded as a special instance corresponding to a degenerate density.

From a Bayesian viewpoint, the listed localization techniques aim at computing one of the following posterior density functions, or an approximation thereof,

$$p(x_t, \mathcal{M} | y_{1:t}, u_{1:t-1}), \quad (1a)$$

$$p(x_t | y_{1:t}, u_{1:t-1}). \quad (1b)$$

Here $u_{1:t-1}$ denotes measurements from potential auxiliary odometric sensors, such as inertial sensors or wheel encoders, used in the localization. Magnetic-field SLAM and map matching aim at computing (1a) and (1b), respectively. Magnetic-field dead reckoning aims to compute an approximation to (1a) using a time-varying map that is accurate in a small neighborhood of the current location.

Before continuing, two remarks should be made. First, the stated densities in (1) correspond to a filtering inference setup, and corresponding densities for a smoothing inference setup can also be defined. Second, since the posterior density function in (1b) can always be calculated from (1a)

via marginalizing over the map \mathcal{M} , the SLAM localization technique is the most general localization technique. As will be shown later, the two other localization techniques can be viewed as special cases of SLAM.

MATHEMATICAL MODELING

The calculation of the posterior densities in (1) is commonly done using recursive application of Bayes' theorem. To that end, a system model for the dynamics of the localization system and the magnetic field measurements of the form

$$p(x_{t+1} | x_t, u_t) \quad (2a)$$

$$p(y_t | x_t, \mathcal{M}) \quad (2b)$$

$$p(x_0) \quad (2c)$$

$$p(\mathcal{M}) \quad (2d)$$

is required. Here, the density in (2a) models the motion dynamics of the localization system, and the likelihood in (2b) models the relationship between the state x_t , the map \mathcal{M} , and the magnetometer measurements y_t at time instant t . Furthermore, the prior densities in (2c) and (2d) capture initial knowledge about the location state x_0 and the map \mathcal{M} . Next, commonly used magnetic field models, magnetometer measurement models, and motion dynamic models will be presented.

Magnetic-field properties

The magnetic field \mathcal{B} has several important properties. Firstly, in linear media, such as air, it is additive and can be decomposed into the nominal Earth magnetic field and local spatial variations, a.k.a anomalies, caused by ferromagnetic materials in the Earth's lithosphere and man-made structures. Secondly, the field is smooth away from sources; its magnitude approximately decays cubically with distance from point sources, and in non-conductive and non-magnetic media, the magnetic field propagates with negligible distortion and similar attenuation to that in a vacuum. Thirdly, from Maxwell's equations, \mathcal{B} is governed by Gauss's law for magnetism, which states that magnetic monopoles do not exist, and the field is therefore divergence-free. Moreover, if the field is static, then in a domain with no magnetized materials or free currents, the Ampère–Maxwell law implies that the field is also curl-free. That is, inside this domain, it holds that

$$\nabla_r \cdot \mathcal{B}(r) = 0 \quad (\text{divergence-free field}), \quad (3a)$$

$$\nabla_r \times \mathcal{B}(r) = 0 \quad (\text{curl-free field}). \quad (3b)$$

Therefore, in a simply connected domain, the static magnetic field can be represented as the gradient of a scalar potential whenever it is curl-free. In this case, the divergence-free condition implies that the potential is harmonic.

Magnetic-field modeling and maps

A variety of mathematical models is used to create maps \mathcal{M} . Examples of widely used models include Gaussian process (GP) approximations, polynomial functions, sums of dipoles, and discrete grid-based function representations [11]. Most of

these models can be abstractly viewed in terms of a basis function expansion of L pre-determined basis functions $\phi_i(r)$, such as radial function bases or polynomial bases. That is, the map is modeled as

$$\mathcal{M}(r) = \Phi^T(r)w = \sum_{\ell=1}^L \phi_\ell^T(r) w_\ell, \quad (4)$$

where

$$\Phi(r) = \begin{bmatrix} \phi_1(r) \\ \vdots \\ \phi_L(r) \end{bmatrix}, \quad w = \begin{bmatrix} w_1 \\ \vdots \\ w_L \end{bmatrix}.$$

Note that (4) is linear in the weights w , but typically nonlinear both in r and in hyperparameters appearing in the basis functions ϕ_i .

The probability density $p(\mathcal{M})$ of the map \mathcal{M} is determined by the probability distribution $p(w)$ of the random weights w . For instance, an approximate GP model is obtained if the weights are normally distributed [12], where the choice of basis functions and weight covariance determines the corresponding covariance kernel of the process. Further, if the weights w are drawn from a degenerated distribution, the model becomes deterministic.

Incorporating curl and divergence properties: There are several ways to incorporate the curl-free and divergence-free properties into the model of the field \mathcal{B} ; if modeling the field magnitude $\|\mathcal{B}\|$, these properties are typically neglected. One approach to enforce the curl-free property is to let the map \mathcal{M} represent a scalar potential, in which case the magnetic field is obtained as its gradient, i.e.,

$$\mathcal{B}(r) = -\nabla_r \mathcal{M}(r). \quad (5)$$

The divergence-free property can be incorporated similarly by noting that the gradient is a linear operator [13, 14]. In this case, the map represents the vector potential. For polynomial function models, both curl- and divergence-free properties can be incorporated straightforwardly [15]. For GP models, this is less common; an exception is presented in [16], where both properties are included. Typically, only the curl-free property is enforced in GP models.

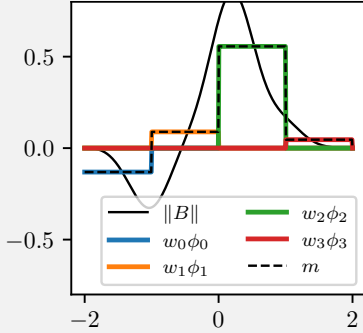
Polynomial functions are ill-suited for large-scale magnetic field modeling due to their poor extrapolation and numerical sensitivity at higher model orders. Consequently, the formulations that are both curl- and divergence-free are primarily used for small-scale magnetic field models, such as those employed in magnetic-field dead reckoning. For large-scale mapping, such as in magnetic-field map matching and SLAM, models that incorporate only the curl-free property, or neither property, are typically adopted.

Other modeling techniques: A range of other magnetic-field map representations cannot be directly expressed in the basis-function expansion form of (4). For instance, neural network-based models that are curl- and divergence-free have been proposed for magnetic-field mapping [14]. Although such models can, in principle, be written as basis function expansions, they are nonlinear in the model parameters and thus fall outside the linear model framework considered here.

Examples of basis function expansions for map modeling

Three commonly used basis function expansions for modeling magnetic field maps \mathcal{M} . In the examples, the map (dashed black line) approximates the magnetic field magnitude $\|B\|$ (solid black line) using four weighted basis functions $\phi_\ell(r)$. The colored lines show the weighted basis functions, i.e., $w_\ell \phi_\ell(r)$.

Grid-based map

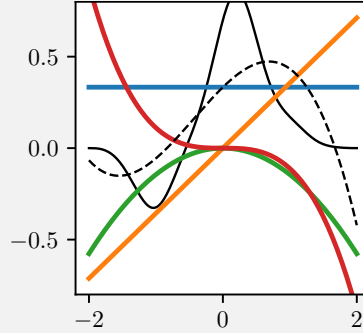


Map approximation using an indicator function basis

$$\phi_\ell(r) = \begin{cases} 1, & r \in \Omega_\ell \\ 0, & \text{otherwise} \end{cases}$$

where Ω_ℓ is the support of the ℓ -th grid cell. Grid-based maps are commonly used in magnetic-field map matching. Due to the discontinuities, this type of map representation can neither encode global curl- nor divergence-free properties of the field.

Polynomial basis map

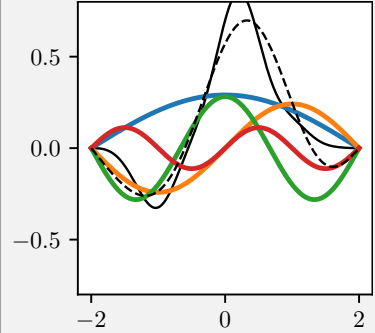


Map approximation using a polynomial basis

$$\phi_\ell(r) = (r - c_\ell)^\ell,$$

where c_ℓ is the center point. Polynomial models are commonly used to construct local-scale maps in magnetic-field dead-reckoning systems. This type of map representation can encode both the curl- and divergence-free properties of the field.

Gaussian process map



Map approximation using a spectral basis

$$\phi_\ell(r) = \cos(2\pi\ell r).$$

Spectral bases can be used to approximate GP kernels and are commonly employed for global-scale magnetic-field maps in SLAM systems. This type of map representation can encode both the curl- and divergence-free properties, but typically only the curl-free property is encoded.

In addition, various non-parametric modeling techniques are frequently employed to model the magnetic field, in which a set of magnetic-field measurements, or features derived from them, is stored to form discrete grid maps; see, e.g., [17]. As the focus of this article is on parametric model-based inference methods, nonparametric modeling techniques will not be further discussed.

where $h(\cdot)$ denotes a function that links the map \mathcal{M} to the expected mean of the measurements. Common functions are:

$$h(x_t, \mathcal{M}) = \begin{cases} C_m^s(q_t) \mathcal{M}(r_t), & \text{if } \mathcal{M} \text{ models the vector field} \\ -C_m^s(q_t) \nabla_r \mathcal{M}(r_t), & \text{if } \mathcal{M} \text{ models the potential field} \\ \mathcal{M}(r_t), & \text{if } \mathcal{M} \text{ models the field magnitude} \end{cases} \quad (6b)$$

Magnetometer measurement models

There exists a range of sensor technologies for measuring the magnetic fields. These can measure either the vector field \mathcal{B} or its magnitude $\|\mathcal{B}\|$. Irrespectively if the vector field or the magnitude is measured, the measurements are typically assumed to be normally distributed and modeled as

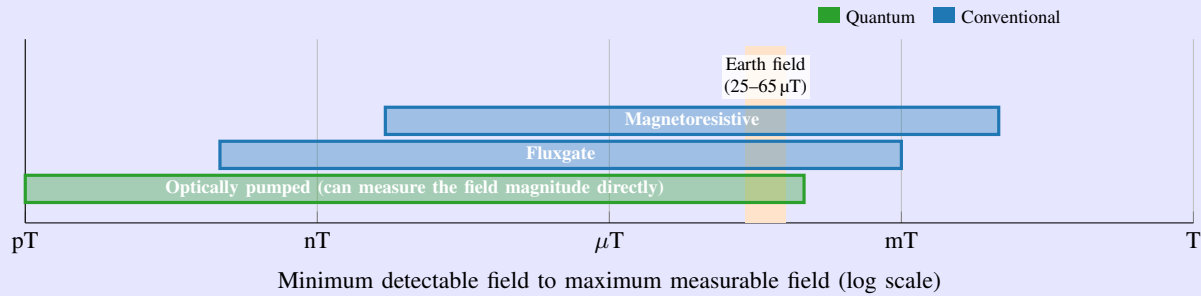
$$p(y_t | x_t, \mathcal{M}) = \mathcal{N}(y_t; h(x_t, \mathcal{M}), R_t). \quad (6a)$$

Here, $C_m^s(q)$ denotes a rotation matrix that transforms a vector from the map coordinate frame to the sensor coordinate frame. In magnetic-field SLAM and map matching, the map coordinate frame is typically the same as the global frame of reference, whereas in magnetic-field dead reckoning, a time-varying frame is used. Furthermore, R_t denotes the covariance of the measurement noise, which is assumed to be uncorrelated across measurement time instants. As highlighted by (6b), if a vector magnetometer is used, then the measurement depends on the orientation q of the magnetometer.

Magnetometer technologies

A wide range of magnetometer technologies based on different physical principles are available, with significant differences in measurement range, size, cost, and power consumption [18, 19]. The technologies also differ in whether they directly measure the magnetic field magnitude or have a specific sensitivity axis. The former are referred to as scalar or total-field magnetometers. In contrast, multiple single-axis sensors can be combined to create a vector magnetometer that measures all components of the vector field. These properties largely determine the suitability of the different technologies for magnetic-field-based localization in indoor and outdoor environments. In the figure below, each box indicates the minimum detectable field and the maximum measurable field for three commonly used magnetometer technologies. The indicated values correspond to compact magnetometer designs suitable for field applications and exclude high-end sensor technologies, such as superconducting quantum interference device (SQUID), which require cooling for superconductivity.

Magnetoresistive sensor technology is employed in contemporary chip-scale vector magnetometers, which are commonly used in indoor magnetic-field localization systems. The fluxgate technology can be used to construct vector magnetometers suitable for both indoor and outdoor localization systems. Fluxgate magnetometers are commonly used to construct magnetometer arrays for indoor magnetic-field dead reckoning (see, e.g., [20]), where the sensitivity of magnetoresistive sensors is insufficient to resolve small spatial variations in the magnetic field over short distances. Optically pumped magnetometers rely on quantum interference effects and offer very high sensitivity, which makes them well-suited for outdoor localization systems. Further, optically pumped magnetometers can be designed to measure the field magnitude directly. This is advantageous outdoors, where spatial variations on the order of nano-Tesla must be resolved against a constant background field of about 50 micro-Tesla. Doing so with a vector magnetometer requires sensor orientation accuracy and sensitivity-axis orthogonality on the order of milli-degrees, which is practically challenging to achieve [19].



Models for the motion dynamics

The motion dynamics of localization systems are defined by the platform on which they are mounted, and no generic motion dynamics model exists. That said, magnetometers are commonly used together with inertial sensors, wheel encoders, and other odometric sensors. The measurements u_t from these sensors can be, but are typically not, treated as measurements in the traditional sense by defining an additional likelihood function analogous to (2b). Instead, they are used as inputs to a deterministic dynamic model

$$x_{t+1} = f(x_t, u_t), \quad (7)$$

which describes a dead reckoning or inertial navigation process; see [25] and [26] for examples of such dynamic models.

To take into account the measurement errors of the sensors, the motion dynamic of the localization system is, based upon a central limit theorem argument, commonly modeled as

$$p(x_{t+1} | x_t, u_t) = \mathcal{N}(x_{t+1}; f(x_t, u_t), Q_t). \quad (8)$$

Here, Q_t is the process noise covariance matrix, which quantifies the effects of sensor errors, as well as numerical

and approximation errors in the dead-reckoning or inertial-navigation process.

There are several reasons for treating the sensor measurements u_t as inputs to the dynamic model and not as traditional measurements via a likelihood function [26]. One reason is that these measurements contain components that are complex to model accurately in a stochastic framework. Another reason is that measurements from these self-contained sensors are continuously available and cannot be disturbed. The dynamic model thereby serves as the backbone of the localization system, ensuring that a localization solution can always be computed, even when magnetometer measurements are unavailable.

STATISTICAL INFERENCE FOR MAP LEARNING

Before examining the inference procedures used in magnetic field-based localization techniques, it is helpful to review the basics about how a map can be inferred from a sequence of magnetometer measurements $y_{1:t}$ collected along a known state trajectory $x_{1:t}$. This is because map learning is a sub-task of both magnetic-field SLAM and magnetic-field dead reckoning.

Magnetometer measurement errors and calibration methods

Magnetometers are affected by intrinsic and extrinsic errors. Intrinsic errors arise from misaligned sensitivity axes, gain imperfections, offsets, and thermal or quantization noise. Extrinsic errors arise from ferromagnetic materials in the sensor housing or the platform carrying the sensor. These are commonly divided into hard-iron effects, caused by permanent magnetic materials, and soft-iron effects, induced by ferromagnetic materials interacting with the Earth's magnetic field; the latter causes an orientation-dependent error. To first order, the combined effects of intrinsic and extrinsic errors can be described by the affine measurement model

$$y_t = A_t(x_t) h(x_t, \mathcal{M}) + b_t + e_t.$$

After calibrating $A_t(\cdot)$ and b_t , if the noise e_t is modeled as normally distributed with covariance R_t , this model is equivalent to the one in (6a).

Several methods exist for calibrating $A_t(\cdot)$ and b_t from a sequence of measurements $y_{1:t}$. They differ in their assumptions about the magnetic field, the state trajectory $x_{1:t}$, and whether the magnetometer coordinate frame must be aligned with the coordinate frames of other sensors in the localization systems, such as inertial sensors. The choice of calibration method also depends on the availability of a calibration rig and on whether $A_t(\cdot)$ and b_t are assumed time-invariant.

A standard approach for calibrating vector magnetometers is ellipsoid fitting [21]. The method exploits the fact that the Euclidean norm of an ideal sensor's measurements is constant if \mathcal{M} is constant in the measurement volume. Since the Euclidean norm is invariant to rotation, the method cannot align the magnetometer coordinate frame with other reference frames. A review of calibration methods utilizing similar assumptions and techniques is given in [22]. Another standard approach for calibrating magnetometers mounted on aircraft, and for compensating permanent, induced, and eddy-current magnetic-field distortions, is based on the Tolles–Lawson model [23]. The model parameters are typically estimated from measurements collected during dedicated calibration maneuvers using least-squares methods.

Many magnetic field localization systems also use auxiliary sensor measurements $u_{1:t}$, such as inertial sensors, when inferring the state x_t . Hence, it is often desirable to jointly calibrate the magnetometer and auxiliary sensors and to align their coordinate frames. To this end, several calibration methods for joint magnetic-field and inertial sensor calibration have been proposed; see, e.g., [24]. Moreover, to avoid dedicated calibration procedures and to handle time-varying sensor errors, recent work has also explored methods for joint state inference and magnetometer calibration [8].

Inferring a map from measurements along a known trajectory is a relatively straightforward inference problem compared to the localization problem addressed later. That said, much research has been conducted on the related, more challenging problem of constructing maps from crowdsourced data when the state trajectory $x_{1:t}$ is not perfectly known. This type of map construction is out of the scope of this article, and the reader is referred to [3] and the references therein.

If a model of the form in (4) is used to represent the map, inferring the map is equivalent to inferring the weight vector w . To that end, assume that the measurements follow (6a) and that the prior on the map $p(\mathcal{M})$, or equivalently, the prior of the weight vector w , is

$$p(\mathcal{M}) \equiv p(w) = \mathcal{N}(w; \mu_{w,0}, P_{ww,0}). \quad (9)$$

The posterior density of the weights w at time t is then

$$p(w | y_{1:t}, x_{1:t}) = \mathcal{N}(w; \mu_{w,t}, P_{ww,t}), \quad (10)$$

where the mean $\mu_{w,t}$ and covariance $P_{ww,t}$ can be computed using the stochastic recursive least-squares equations [27]

$$\mu_{w,t} = \mu_{w,t-1} + K_t (y_t - H_t \mu_{w,t-1}), \quad (11a)$$

$$P_{ww,t} = (\mathcal{I} - K_t H_t^\top) P_{ww,t-1}, \quad (11b)$$

$$K_t = P_{ww,t-1} H_t^\top (H_t P_{ww,t-1} H_t^\top + R_t)^{-1}. \quad (11c)$$

where

$$H_t \triangleq h(x_t, \Phi^\top(r_t)). \quad (11d)$$

The posterior density of the map at location r_* is finally given by

$$p(\mathcal{M}(r_*) | y_{1:t}, x_{1:t}) = \mathcal{N}(\Phi^\top(r_*) \mu_{w,t}, \Phi^\top(r_*) P_{ww,t} \Phi(r_*)). \quad (12)$$

Next, the important task of selecting the hyperparameter in the model used to construct the map will be discussed.

Hyperparameter selection

To accurately infer the map \mathcal{M} , the hyperparameters in the model (4) must be properly tuned. Important hyperparameters include the number of basis functions N_p , the prior mean $\mu_{w,0}$ and covariance $P_{ww,0}$ of the weights w , and parameters that determine the spatial properties of the basis functions $\phi_\ell(x)$, such as the length scale in radial basis functions. These hyperparameters determine the resolution and spatial variability of the inferred map. Hyperparameters can be learned from data by maximizing the log-marginal likelihood [28]. In practice, they are frequently set to physically motivated values, especially when the map is inferred recursively.

The number of basis functions N_p required to accurately represent the magnetic field depends on both the desired spatial resolution and the spatial extent of the map. For

small-scale models, N_p can be selected using standard model-order selection criteria, such as the Akaike information criterion [29]. For large-scale maps, including GP- and grid-based representations, N_p is typically selected empirically to achieve the desired accuracy over the coverage area.

The number of basis functions also directly impacts the computational complexity of the map inference. This is particularly critical for GP-based models, where the computational complexity of inference scales cubically with the number of basis functions N_p . To limit computational complexity, large-scale maps are sometimes represented using multiple smaller-scale maps [10] or approximated using local or sparse GP formulations [11, 30].

STATISTICAL INFERENCE FOR LOCALIZATION

As previously stated, from a Bayesian perspective, the localization techniques magnetic-field map matching, SLAM, and dead reckoning aim to compute either of the posterior densities in (1). Next, starting from the Bayesian filter recursions for magnetic-field SLAM, it is shown that from a theoretical viewpoint, magnetic-field map matching and dead reckoning can be viewed as special cases of the magnetic-field SLAM inference problem. Thereafter, common implementation approaches and aspects of the three localization techniques are described.

Before continuing, recall that the map \mathcal{M} , as defined by the basis function representation in (4), is fully parameterized by the weights w . With this representation, the posterior, likelihood, and prior can be written equivalently as $p(x_t, w | y_{1:t}, u_{1:t-1})$, $p(y_t | x_t, w)$, and $p(w)$, respectively. This notation is used hereafter.

The posterior densities for magnetic-field SLAM in (1a) can, for $t > 0$, be calculated using the system models in (2) and the Bayesian filter recursions [31]

$$p(x_t, w | y_{1:t}, u_{1:t-1}) \propto p(y_t | x_t, w)p(x_t, w | y_{1:t-1}, u_{1:t-1}), \quad (13a)$$

$$p(x_t, w | y_{1:t-1}, u_{1:t-1}) = \int p(x_t | x_{t-1}, u_{t-1}) \cdot p(x_{t-1}, w | y_{1:t-1}, u_{1:t-2}) dx_{t-1}, \quad (13b)$$

where the initial conditions for $t = 0$ are given by the prior densities in (2c) and (9). The connection between the SLAM inference problem and the earlier presented map inference problem can be seen by factorizing the SLAM posterior density as follows

$$\begin{aligned} p(x_t, w | y_{1:t}, u_{1:t-1}) &= \int p(x_t, x_{1:t-1}, w | y_{1:t}, u_{1:t-1}) dx_{1:t-1} \\ &= \underbrace{\int p(w | x_{1:t}, y_{1:t})}_{\text{Map inference}} \underbrace{p(x_{1:t} | y_{1:t}, u_{1:t-1})}_{\text{State inference}} dx_{1:t-1}. \end{aligned} \quad (14)$$

This factorization highlights that magnetic-field SLAM consists of a coupled state- and map-inference problem. Given a trajectory posterior, the map posterior is obtained by conditioning on the entire state history. Marginalizing past states in the inferred trajectory recovers the SLAM posterior density.

Magnetic-field map matching can be seen as a special case of (13), where the posterior density in (1b) can be calculated by, at every time instant t , marginalizing the posterior density with respect to the weights w . This is not how magnetic-field map matching is implemented in practice, as it would require inferring the weights w , which is computationally expensive. Instead, in magnetic-field map-matching, it is assumed that prior knowledge of the map is sufficient for accurate localization. Therefore, the new information in the measurements $y_{1:t}$ and the trajectory $x_{1:t}$ about the map is neglected to make the approximation $p(w | x_{1:t}, y_{1:t}) \approx p(w)$, which, if inserted in (14), results in the approximation

$$p(x_t, w | y_{1:t}, u_{1:t-1}) \approx p(w)p(x_t | y_{1:t}, u_{1:t-1}). \quad (15)$$

Next, inserting this approximation into (13) and marginalizing with respect to the weights w , i.e., the map \mathcal{M} , yields the magnetic-field map-matching inference recursions

$$\begin{aligned} p(x_t | y_{1:t}, u_{1:t-1}) &\propto \int p(y_t | x_t, w)p(w) dw \\ &\quad \cdot p(x_t | y_{1:t-1}, u_{1:t-1}) \end{aligned} \quad (16a)$$

$$\begin{aligned} p(x_t | y_{1:t-1}, u_{1:t-1}) &\approx \int p(x_t | x_{t-1}, u_{t-1}) \\ &\quad \cdot p(x_{t-1} | y_{1:t-1}, u_{1:t-2}) dx_{t-1} \end{aligned} \quad (16b)$$

From (16a) it can be seen that in the map matching done via the likelihood $p(y_t | x_t, w)$, the uncertainty about the map is taken into account by marginalizing over w . If the map is a deterministic function, no marginalization is needed, further reducing computational complexity.

Also, magnetic-field dead reckoning can be seen as a special case of magnetic-field SLAM. In this case, the computational complexity of inferring the map \mathcal{M} is reduced by instead using a time-varying map \mathcal{M}_t that only describes the magnetic field (or its magnitude) accurately in a small region around the current location x_t . Since the map only needs to be accurate in a small region around the current locations, only a few basis function weights are needed to represent the map, saving memory and reducing computational complexity. Using the time-varying map \mathcal{M}_t , equivalently defined by the weights w_t , the magnetic-field SLAM posterior density is approximated as

$$p(x_t, w | y_{1:t}, u_{1:t-1}) \approx p(x_t, w_t | y_{1:t}, u_{1:t-1}). \quad (17)$$

Further, the dynamics of the time-varying map \mathcal{M}_t are modeled by the Markov transition density

$$p(w_{t+1} | w_t, x_t, u_t), \quad (18)$$

which captures the translation and rotation of the map with the state x_t ; the map is typically expressed in the sensor coordinate frame. With this approximate posterior density and dynamics for the time-varying map, the resulting Bayesian filter recursions for magnetic-field dead reckoning for $t > 1$ become

$$\begin{aligned} p(x_t, w_t | y_{1:t}, u_{1:t-1}) &\propto p(y_t | x_t, w_t)p(x_t, w_t | y_{1:t-1}, u_{1:t-1}) \end{aligned} \quad (19a)$$

$$\begin{aligned}
& p(x_t, w_t \mid y_{1:t-1}, u_{1:t-1}) \\
&= \iint p(w_t \mid w_{t-1}, x_{t-1}, u_{t-1}) p(x_t \mid x_{t-1}, u_{t-1}) \\
&\quad \cdot p(x_{t-1}, w_{t-1} \mid y_{1:t-1}, u_{1:t-2}) dw_{t-1} dx_{t-1}. \quad (19b)
\end{aligned}$$

Here the initial conditions at $t = 0$ are given by (2c) and the prior density of the local map $p(w_0)$. In the recursion, at each time step, the previous weights w_{t-1} are marginalized. Although the marginalization over w_{t-1} increases the per-step computational cost, this is outweighed by the substantial reduction in complexity obtained by representing the map with a low-dimensional parameter vector w_t instead of the weight vector w used in magnetic-field SLAM. The price paid for the lower computational complexity is that no long-term global map is constructed, hence no loop closure can be performed. As a result the location error grows without bound. More details and views on the connection between magnetic-field SLAM and dead-reckoning are presented in [32].

To summarize, magnetic-field map matching and dead reckoning can be viewed as special cases of magnetic-field SLAM, in which approximations are introduced to reduce computational complexity or memory requirements. Consequently, these three localization techniques share a set of common inference and implementation challenges.

The inference process for all three localization techniques is nonlinear and must be solved using nonlinear filtering methods, such as the extended Kalman filter (EKF), unscented Kalman filter (UKF), and particle filter (PF), or nonlinear optimization-based methods, such as factor-graph-based optimization (FGO). Further, if the orientation q is a part of the state x , the fact that orientations belong to the Lie group of rotations must be taken into account in the inference process.

Further, in magnetic-field SLAM and map matching, the posterior distributions are often multi-modal when the dynamic model $p(x_{t+1} \mid x_t, u_t)$ or the prior $p(x_0)$ is insufficiently informative. This behavior stems from the limited information content in a single magnetometer measurement; even in the absence of noise, a single measurement is generally insufficient to uniquely identify a location at a global scale. To handle the multi-modality, PFs techniques are frequently employed for magnetic-field SLAM and map-matching.

Magnetic-field map matching

Magnetic-field map matching is used both for indoor and outdoor applications. Indoors, 2D or full 3D spatial maps of the magnetic field magnitude or vector field are assumed to be constructed from one or several surveying campaigns. For outdoor applications, scalar maps are available, such as the Earth Magnetic Anomaly Grid¹. Methods that directly fit the Bayesian recursions from (16) are, e.g., [35–37].

An alternative, commonly used approach for magnetic-field map matching is closer to fingerprinting in robotics and matches time sequences of magnetic measurements with existing maps, see e.g., [17, 38–41]. These methods can be used in the presented Bayesian framework by extending the

Inference of states including orientations

If the orientation q is part of the state x , the inference problem involves a non-Euclidean space, since orientations belong to the Lie group of rotations. As a consequence, several operations used by standard nonlinear filtering techniques, such as the EKF and UKF, do not apply directly. For example, orientation errors cannot be added linearly to the state estimate. Therefore, these filters cannot be directly applied to states that include orientation components q . In practice, this is typically handled by decomposing the orientation q into a nominal part \bar{q} and an error part ϵ , where the error ϵ is defined in a Euclidean space to which standard filtering techniques can be applied [26]; the nominal state is maintained on the rotation manifold. This principle underlies commonly used invariant and error-state Kalman filtering techniques [33, 34].

measurement model (6a) to represent a sequence of measurements. However, the maps used are typically nonparametric and therefore do not fit the description from (4).

The challenge with inference for localization using an existing magnetic map is the multimodality of the posterior due to the non-uniqueness of the magnetic field. This is illustrated in Fig. 2, which shows that each measurement typically matches with several locations in the map. Without an accurate prior on the initial location, a unique location can therefore only be inferred over time, after sufficient movement of the localization system. Multimodality is also of concern when the dynamic model is inaccurate or in regions with limited spatial variations.

The map-matching inference problem (16) has been addressed using PF and EKF-based approaches. Note that although these latter approaches can not represent multimodal posteriors, the inference problem becomes unimodal once sufficient prior information and an accurate enough dynamic model are available.

The accuracy of these methods for localization using an existing map depends on the amount of variation in the magnetic field and will therefore also vary spatially and be highly dependent on the environment. See also [42], where a Bayesian Cramér-Rao lower bound has been derived for magnetic field map matching-based localization. Estimation accuracy can degrade when the true posterior is multi-modal and an algorithm such as an EKF is used, which can only track a single mode. Furthermore, magnetometer calibration is essential for magnetic-field map matching localization to avoid mismatches between the measurements during the localization process and the measurements used to create the map. Because of this, recent work has explored simultaneous localization and calibration [8].

Magnetic-field SLAM

As of today, the main application of magnetic-field SLAM is indoor localization, see e.g., [10, 36, 43, 44]. That said,

¹<https://www.ngdc.noaa.gov/products/earth-magnetic-model-anomaly-grid-2>

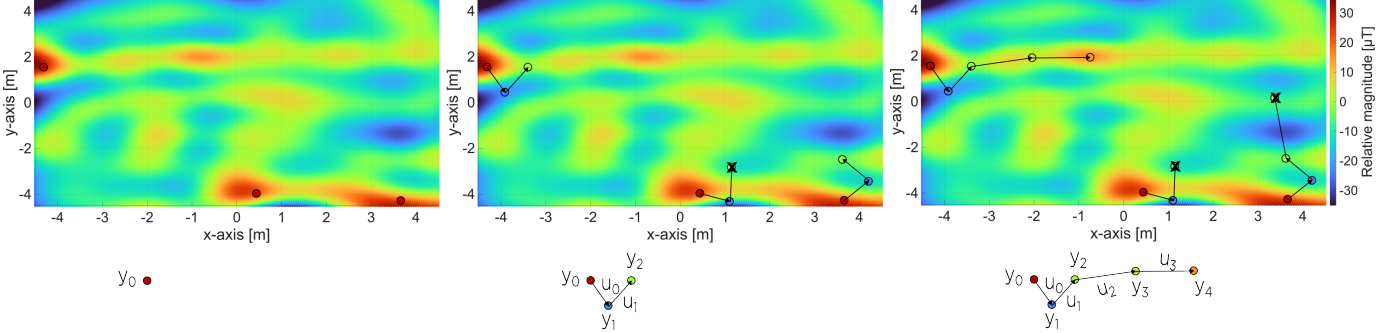


Fig. 2: Illustration of localization using magnetic-field map-matching. The inference algorithm alternates between comparing the magnetometer measurement y_t to the map \mathcal{M} and predicting the next state x_{t+1} using the motion dynamics $p(x_{t+1} | x_t, u_t)$. The graph below each image shows the dead reckoning (edges) and measurement (nodes) information available at that point.

outdoor applications also exist; see, e.g., the aerial magnetic-field SLAM system in [45]. A stochastic treatment of the map is particularly important in magnetic-field SLAM, since the map uncertainty must be accounted for during exploration of previously unmapped areas, while mapped regions can be exploited for localization during revisits. Consequently, many existing works represent the magnetic field map using GPs.

Most existing work on magnetic-field SLAM directly fits the recursions (13). Nevertheless, there are notable exceptions, see e.g. [46–49], that match measurement sequences in a similar manner to magnetic-field map-matching approaches in [17, 38]. After matching the measurement sequences, these SLAM methods conduct an explicit loop closure. This is achieved by substituting the measurement likelihood in (6a) with a loop-closure likelihood that imposes the pseudo-measurement $r_t \approx r_{t-\tau}$, where $t - \tau$ denotes a past time instant, which, according to the measurement sequence matching procedure, corresponds to the same physical location as the current time instant t .

Although the magnetic-field SLAM inference problem can be solved using standard nonlinear inference techniques, challenges arise from its high dimensionality. While $\dim(x_t)$ is typically on the order of ten, the number of basis functions w that is needed to accurately represent the magnetic field in large-scale environments is typically on the order of thousands or more. Therefore, computational complexity is often a limiting factor in magnetic-field SLAM. Unless the basis functions from (4) have finite support, there is no sparsity that can be exploited in the Bayesian recursions. Potentially because of this, while FGO is used for magnetic-field SLAM that matches measurement sequences and includes explicit loop closures [48–50], existing work solving the inference problem (13) focuses on EKFs [43], and PF methods [10, 51]. Note that, for particle methods, the state dimension appears prohibitive. However, since the inference of the basis function weights w is a linear estimation problem (see (11)), it is possible to use a Rao-Blackwellized, a.k.a. marginalized, PF [10, 51]. These only represent the state x_t using particles, while every particle infers its own map w using (11).

The accuracy of magnetic-field SLAM methods inherently depends on the frequency of revisiting previous locations, the amount of magnetic-field variation, and the accuracy of the

dynamic model. If previous locations are not revisited for extended periods or when the dynamic model is inaccurate, the large uncertainty in the state estimates prevents effective correction of location estimates during revisits. In addition, the measurement likelihood is directly affected by magnetometer calibration errors, which in turn limit the achievable localization accuracy. To address this issue, recent work has investigated joint magnetometer calibration and magnetic-field SLAM [52].

Dead reckoning

As of today, most magnetic-field dead reckoning methods have been developed for pedestrian localization in indoor environments [20, 53–55]. Only a limited amount of work on magnetic-field dead reckoning for outdoor applications exists, with two examples being train localization [56] and autonomous underwater vehicle localization [57]. This may be attributed to the fact that indoor magnetic fields exhibit significant spatial variations over short length scales, whereas outdoor magnetic fields do not. Consequently, magnetic-field dead reckoning outdoors is more challenging and more sensitive to temporal variations in the magnetic field [57]. Notably, most magnetic-field dead reckoning methods use measurements from an array of magnetometers, such as the one shown in Fig. 3, to make the likelihood sufficiently informative for reliable localization. That is, $p(y_t | w_t, x_t)$ in (19) is replaced by

$$\prod_{n=1}^N p(y_t^{(n)} | x_t, w_t), \quad (20)$$

where $y_t^{(n)}$ denotes the measurement from the n^{th} magnetometer and N is the total number of magnetometers in the array.

Although recent state-of-the-art methods are based on the Bayesian recursions presented in (19), the idea of magnetic-field dead reckoning was earlier approached via the differential equation [58]

$$\dot{\mathcal{B}}(r) = \mathcal{B}(r) \times \omega + \nabla_r \mathcal{B}(r) v. \quad (21)$$

Equation (21) shows that, if the time derivative of the magnetic field $\dot{\mathcal{B}}(r)$, its spatial Jacobian $\nabla_r \mathcal{B}(r)$, and the angular rate ω are measured, the velocity v can be inferred; all quantities

are here expressed in the magnetometer coordinate frame. An estimate of the spatial Jacobian of the magnetic field can be obtained from measurements of an array of vector magnetometers, such as the planar array shown in Fig. 3. Notably, if the field is assumed to be curl- and divergence-free, a planar array of vector magnetometers is sufficient to recover the full three-dimensional spatial Jacobian of the field [15]. By integrating the inferred velocity and the measured angular rate over time, magnetic-field dead reckoning can be performed. However, in practice, the inferred velocity is more commonly used to aid an inertial navigation system [54, 55].

More recently, the magnetic-field dead reckoning problem has also been approached from a model-learning perspective [15, 29]. This approach is illustrated in Fig. 3, where a local time-varying magnetic field model \mathcal{M}_t , parameterized by w_t , is fitted to the array measurements from two consecutive time instants. The displacement Δr_t and orientation change Δq_t of the array between t and $t+1$ are treated as unknown parameters and inferred jointly with the parameters of the magnetic field model. Specifically, the posterior density

$$p(\Delta r_t, \Delta q_t, w_t | y_t^{(1)}, \dots, y_t^{(N)}, y_{t+1}^{(1)}, \dots, y_{t+1}^{(N)}) \propto p(w_t) \cdot p(\Delta r_t, \Delta q_t) \prod_{n=1}^N p(y_t^{(n)} | x_t, w_t) p(y_{t+1}^{(n)} | x_{t+1}, w_t), \quad (22a)$$

where $x_t = 0$ and

$$x_{t+1} = \begin{bmatrix} \Delta r_t + C_s^m(\Delta q_t) d^{(n)} \\ \Delta q_t \end{bmatrix}, \quad (22b)$$

is inferred. Here, $d^{(n)}$ denotes the location of the n^{th} magnetometer in the array, expressed in the sensor coordinate frame, and $p(\Delta r_t, \Delta q_t)$ represents prior information about the displacement and orientation change. By accumulating the inferred displacements Δr_t and orientation changes Δq_t over time, dead reckoning can be performed. Notably, unlike the differential-equation-based approach, the model-learning approach can be applied to both vector and total-field magnetometers.

Current state-of-the-art methods for magnetic-field dead reckoning implement the Bayesian filter recursions in (19) using an error-state Kalman filter, in which the posterior is approximated as normally distributed [20, 53]. A first-order curl- and divergence-free polynomial map \mathcal{M}_t is typically used to represent the field. As these implementations use arrays holding many magnetometers, careful calibration to align the coordinate axes and the sensitivities of all magnetometers is required for the methods to work well.

As presented earlier, the Bayesian recursions for magnetic-field dead reckoning in (19) can be viewed as a special case of magnetic-field SLAM with a local time-varying map \mathcal{M}_t defined by the weights w_t . They can also be interpreted as a recursive extension of the model-learning approach in (22a) to magnetic-field dead reckoning, in which a dynamic model of the form (18) is introduced to describe the evolution of the local time-varying map \mathcal{M}_t . From a SLAM perspective, the fact that the local map \mathcal{M}_t is accurate only in the vicinity of the current state and has finite memory due to the dynamics of the weights w_t implies that no long-term magnetic-field

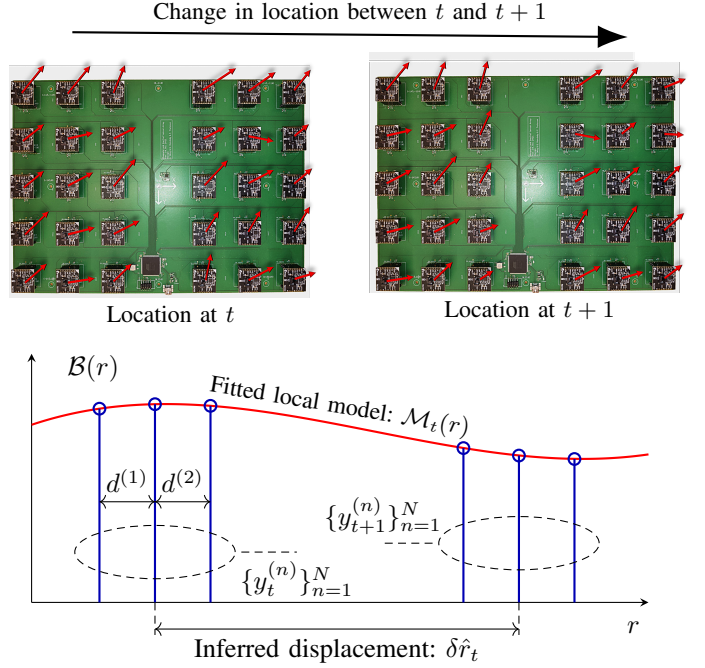


Fig. 3: At top, an array with 30 vector magnetometers measuring the magnetic field at two consecutive locations. Below, a conceptual illustration in 1D of how the displacement Δr_t can be inferred by fitting a local magnetic field model \mathcal{M}_t to the measurement from the two locations, and treating the displacement Δr_t as an unknown parameter in the model.

memory can be exploited. Consequently, loop closure as in magnetic-field SLAM is not possible, and the localization error grows without bound. Conversely, when a magnetic-field SLAM system is provided with measurements from a magnetometer array, it effectively behaves as a magnetic-field dead reckoning system during exploration of previously unmapped areas [32]. Hence, if inertial navigation is used as the backbone of the SLAM process, this substantially reduces the growth rate of the location error when new areas are mapped and extends the feasible exploration duration; typically, the growth rate of the inertial navigation system localization error is reduced from cubic to linear in time.

Currently, no performance bounds on magnetic-field dead reckoning exist. However, a Cramér-Rao lower bound on the displacement (velocity) using the model-learning approach was derived in [15] and [56], assuming a polynomial and Gaussian process map, respectively. The bound in [15] showed that, if the magnetic field can be locally approximated by a first-order polynomial, the estimation accuracy is inversely proportional to the slope-to-noise ratio and the square of the array length. Recently, a similar Cramér-Rao lower bound that also considers the temporal variations in the field was derived. The bound shows that for outdoor magnetic-field dead reckoning, the temporal variations have a significant effect on the accuracy, often surpassing the effect of sensor noise [57].

CHALLENGES AND OUTLOOK

While research to date has demonstrated the feasibility of using spatial variations in the magnetic field for localization, many signal-processing challenges remain before these localization systems can be commercially deployed at scale. Moreover, advances in quantum magnetometer sensor technology are enabling the manufacture of highly sensitive, small-form-factor, low-power sensors, with noise levels on the order of $\text{pT}/\sqrt{\text{Hz}}$. As SQUID-based magnetometer technology continues to mature and transition toward commercial localization applications, sensor sensitivity and noise performance are expected to improve further. For many localization applications, this implies that sensor noise is no longer the dominant source of error. Instead, errors due to model imperfections, unmodeled platform disturbances, and inference approximations increasingly dominate, which calls for more advanced signal-processing methods for modeling, calibration, and inference.

Currently, there is a lack of theoretical and analytically interpretable bounds on the achievable localization accuracy for magnetic-field SLAM and magnetic-field dead reckoning; such bounds exist for magnetic-field map-matching, see e.g., [42]. In addition, observability analyses characterizing the conditions under which system states, calibration parameters, and magnetic-field map parameters can be inferred are largely missing. Consequently, it remains difficult to analyze trade-offs in sensor and system designs and configurations, as well as the role of trajectory and motion excitation in the inference process. Such bounds and observability analysis results are also required when magnetic-field-based localization is to be combined with path and motion planning, where localization performance must be predicted as a function of the planned path and motion.

Scalability and computational efficiency remain a key bottleneck, especially when aiming for real-time estimation. Current map and state inference techniques for magnetic-field SLAM are computationally demanding, and scaling these to large environments is still a challenge [10, 11]. Here, recent advances in sparse GP approximations, distributed GP regression, and scalable Bayesian inference methods may offer solutions. However, research is needed to adapt these techniques to handle the nonlinearities and the multimodal probability distributions characteristic of magnetic-field localization.

Several publicly available datasets and open-source implementations for magnetic-field localization exist, see e.g., [20, 28, 38, 43, 47, 51]. Notably, these publications are almost exclusively focused on indoor localization. For outdoor applications, global and regional magnetic field databases, such as the Earth Magnetic Anomaly Grid, provide magnetic field data and maps that may be used for map-matching localization. That said, publicly available datasets combining magnetic measurements with ground-truth trajectories for outdoor and large-scale scenarios remain scarce, hindering benchmarking and reproducibility.

Map construction and maintenance remain challenging in many application domains. National institutes frequently conduct surveys to create maps of the Earth's magnetic field, which may be used for map-matching in aerospace and

on-surface applications [7]. However, with current methods, the Earth's magnetic field can only be reliably extrapolated upwards, away from the Earth's surface, and not downwards. Hence, it is challenging to directly use these maps in subsurface applications, and new modeling and extrapolation techniques are needed.

The map maintenance challenges are further compounded by temporal variations in the ambient magnetic field. In outdoor magnetic-field localization of high-velocity platforms, the spatial variations appear as a high-frequency component that can be separated from low-frequency temporal variations. However, for slow-moving platforms, the spatial and temporal field components cannot be separated, and correction data from a reference sensor is typically required. Alternatively, for magnetic-field map-matching localization, gradient-based map matching using magnetometer arrays may be used [59]. The use of magnetic-field gradients in magnetic-field SLAM remains largely unexplored.

Current methods for indoor magnetic-field localization that exploit spatial variations in the magnetic field typically neglect temporal field variations. While temporal variations in the Earth's magnetic field can often be neglected indoors, changes in building layouts, furniture, or equipment may cause abrupt changes in the spatial field, leading to erroneous maps. How to detect, model, and adapt to such changes remains largely unexplored [28].

At a system level, multiple challenges exist. Disturbances from the platform on which the localization system is mounted pose a significant challenge to the practical deployment of magnetic-field-based localization. Classical disturbance cancellation methods, such as Tolles–Lawson-type models for compensating aircraft-induced magnetic interference, are becoming insufficient as sensor performance increases. Here, machine-learning-based disturbance modeling and compensation methods have the potential to play an important role, see e.g., [60].

In magnetic-field SLAM, access to accurate dead reckoning or inertial navigation is fundamental to enable extended exploration phases in which new areas are mapped. Contemporary consumer-grade inertial sensors generally lack the accuracy required to enable practically usable magnetic-field SLAM systems for indoor localization. Recent research indicates that magnetic-field SLAM using arrays of magnetometers, thereby inheriting properties of magnetic-field dead reckoning, may offer a potential solution [32].

Another system-level challenge, extending beyond magnetic-field-based localization, is the need for methods to monitor the consistency and integrity of the inferred localization information. To date, most research on magnetic-field-based localization has focused on maximizing the accuracy of inferred point estimates of the location. However, consistency and integrity monitoring are fundamental if the localization information is to be used in control and decision-making systems.

Finally, the signal-processing principles, methods, and algorithms developed for magnetic-field localization have the potential to transfer to other physical fields. For example, gravity-based and terrain-based navigation share many characteristics

with magnetic-field localization and could benefit from similar modeling and inference techniques.

ACKNOWLEDGMENT

This work has been partially funded by the Swedish Research Council project 2020-04253 *Tensor-field based localization* and Vinnova, Sweden's Innovation Agency, and Swedish Armed Forces, project 2025-03855 *Electromagnetic navigation for smaller unmanned underwater vehicles*. This work was also partially performed within the Competence Center SEDDIT (Sensor Informatics and Decision making for the DIgital Transformation), supported by Sweden's Innovation Agency within the research and innovation program Advanced digitalization. This work was also supported by the Sensor AI Lab through the AI Labs Program of the Delft University of Technology.

REFERENCES

- [1] B. Li, T. Gallagher, A. G. Dempster, and C. Rizos, "How feasible is the use of magnetic field alone for indoor positioning?" in *Proceedings of International Conference on Indoor Positioning and Indoor Navigation (IPIN)*, Sydney, Australia, Nov. 2012, pp. 1–9.
- [2] M. Muradoglu, M. T. Johnsson, N. M. Wilson, Y. Cohen, D. Shin, T. Navickas, T. Pyragius, D. Thomas, D. Thompson, S. I. Moore *et al.*, "Quantum-assured magnetic navigation achieves positioning accuracy better than a strategic-grade INS in airborne and ground-based field trials," *arXiv:2504.08167*, 2025.
- [3] G. Ouyang and K. Abed-Meraim, "A survey of magnetic-field-based indoor localization," *Electronics*, vol. 11, no. 6, 2022.
- [4] V. Pasku, A. De Angelis, G. De Angelis, D. D. Arumugam, M. Dionigi, P. Carbone, A. Moschitta, and D. S. Ricketts, "Magnetic field-based positioning systems," *IEEE Communications Surveys and Tutorials*, vol. 19, no. 3, pp. 2003–2017, 2017.
- [5] W. Lei, C. Zhang, Z. Jin, and J. Chen, "A review on magnetic-assisted localization for mobile robots," *Measurement*, p. 116643, 2025.
- [6] S. He and K. G. Shin, "Geomagnetism for smartphone-based indoor localization: Challenges, advances, and comparisons," *ACM Computing Surveys (CSUR)*, vol. 50, no. 6, pp. 1–37, 2017.
- [7] F. Goldenberg, "Geomagnetic navigation beyond the magnetic compass," in *Proc. of IEEE/ION PLANS*, San Diego, CA, Apr. 2006, pp. 684–694.
- [8] B. Siebler, A. Lehner, S. Sand, and U. D. Hanebeck, "Simultaneous localization and calibration (SLAC) methods for a train-mounted magnetometer," *NAVIGATION: Journal of the Institute of Navigation*, vol. 70, no. 1, 2023.
- [9] M. Angermann, M. Frassl, M. Doniec, B. J. Julian, and P. Robertson, "Characterization of the indoor magnetic field for applications in localization and mapping," in *Proceedings of International Conference on Indoor Positioning and Indoor Navigation (IPIN)*, Sydney, Australia, Nov. 2012, pp. 1–9.
- [10] M. Kok and A. Solin, "Scalable magnetic field SLAM in 3D using Gaussian process maps," in *Proceedings of 21th IEEE International Conference on Information Fusion (FUSION)*, Cambridge, UK, Jul. 10–13 2018, pp. 1353–1360.
- [11] F. M. Viset, R. Helmons, and M. Kok, "Spatially scalable recursive estimation of Gaussian process terrain maps using local basis functions," *IEEE Transactions on Signal Processing*, vol. 73, pp. 1444–1453, Mar. 2025.
- [12] A. Solin and S. Särkkä, "Hilbert space methods for reduced-rank gaussian process regression," *Statistics and Computing*, vol. 30, no. 2, pp. 419–446, Aug. 2020.
- [13] C. Jidling, N. Wahlström, A. Wills, and T. B. Schön, "Linearly constrained Gaussian processes," *Advances in Neural Information Processing Systems*, vol. 30, 2017.
- [14] U. H. Coskun, B. Sel, and B. Plaster, "Magnetic field mapping of inaccessible regions using physics-informed neural networks," *Scientific Reports*, vol. 12, no. 1, Jul. 2022.
- [15] I. Skog, G. Hendeby, and F. Gustafsson, "Magnetic odometry-a model-based approach using a sensor array," in *Proceedings of 21th IEEE International Conference on Information Fusion (FUSION)*, Cambridge, UK, Jul. 10–13 2018, pp. 794–798.
- [16] N. Wahlström, M. Kok, T. B. Schön, and F. Gustafsson, "Modeling magnetic fields using Gaussian processes," in *Proceedings of the 38th International Conference on Acoustics, Speech, and Signal Processing (ICASSP)*, Vancouver, Canada, May 2013, pp. 3522–3526.
- [17] K. P. Subbu, B. Gozick, and R. Dantu, "Indoor localization through dynamic time warping," in *Proceedings of the IEEE International Conference on Systems, Man, and Cybernetics*, Anchorage, AK, Oct. 2011, pp. 1639–1644.
- [18] J. E. Lenz, "A review of magnetic sensors," *Proceedings of the IEEE*, vol. 78, no. 6, pp. 973–989, Jun. 1990.
- [19] A. Edelstein, "Advances in magnetometry," *Journal of Physics: Condensed Matter*, vol. 19, no. 16, p. 165217, Apr. 2007.
- [20] C. Huang, G. Hendeby, H. Fourati, C. Prieur, and I. Skog, "MAINS: A magnetic-field-aided inertial navigation system for indoor positioning," *IEEE Sensors Journal*, vol. 24, no. 9, pp. 15 156–15 166, Mar. 2024.
- [21] V. Renaudin, M. H. Afzal, and G. Lachapelle, "Complete triaxis magnetometer calibration in the magnetic domain," *Journal of Sensors*, vol. 2010, no. 1, Dec. 2010.
- [22] K. Papafotis, D. Nikitas, and P. P. Sotiriadis, "Magnetic field sensors' calibration: Algorithms' overview and comparison," *Sensors*, vol. 21, no. 16, Aug. 2021.
- [23] Q. Han, Z. Dou, X. Tong, X. Peng, and H. Guo, "A modified tolles–lawson model robust to the errors of the three-axis strapdown magnetometer," *IEEE Geoscience and Remote Sensing Letters*, vol. 14, no. 3, pp. 334–338, Mar. 2017.
- [24] M. Kok and T. B. Schön, "Magnetometer calibration using inertial sensors," *IEEE Sensors Journal*, vol. 16, no. 14, pp. 5679–5689, 2016.
- [25] M. Kok, J. D. Hol, and T. B. Schön, "Using inertial sensors for position and orientation estimation," *Foundations and Trends on Signal Processing*, vol. 11, no. 1–2, pp. 1–153, 2017.
- [26] J. A. Farrell and M. Barth, *The Global Positioning System and Inertial Navigation*. New York, NY, USA: McGraw-Hill, 1998.
- [27] T. Kailath, A. H. Sayed, and B. Hassibi, *Linear Estimation*. Upper Saddle River, NJ: Prentice Hall, 2000.
- [28] A. Solin, M. Kok, N. Wahlström, T. B. Schön, and S. Särkkä, "Modeling and interpolation of the ambient magnetic field by gaussian processes," *IEEE Transactions on Reliability*, vol. 34, no. 4, pp. 1112–1127, Jun. 2018.
- [29] I. Skog, G. Hendeby, and F. Trulsson, "Magnetic-field based odometry — An optical flow inspired approach," in *Proceedings of International Conference on Indoor Positioning and Indoor Navigation (IPIN)*, Lloret de Mar, Spain, Nov. 29–Dec. 2 2021.
- [30] I. Abdul-Raouf, V. Gay-Bellile, S. Bourgeois, and A. Paljic, "Large scale mapping of indoor magnetic field by local and sparse Gaussian processes," in *Proceedings of the 8th Annual Conference on Robot Learning (CoRL)*, Munich, Germany, Nov. 2024.
- [31] H. Durrant-Whyte and T. Bailey, "Simultaneous localization and mapping: part I," *IEEE Robotics and Automation Magazine*, vol. 13, no. 2, pp. 99–110, Jun. 2006.
- [32] I. Skog, M. Kok, G. Hendeby, C. Huang, and T. Edridge, "On the connection between magnetic-field odometry aided inertial navigation and magnetic-field SLAM," in *Proceedings of IEEE/ION Position, Location and Navigation Symposium (PLANS)*, Salt-Lake City, UT, May 2025.
- [33] A. Barrau and S. Bonnabel, "The invariant extended Kalman filter as a stable observer," *IEEE Transactions on Automatic Control*, vol. 62, no. 4, pp. 1797–1812, 2016.
- [34] J. Sola, "Quaternion kinematics for the error-state Kalman filter," *arXiv:1711.02508*, 2017.
- [35] A. Solin, S. Särkkä, J. Kannala, and E. Rahtu, "Terrain navigation in the magnetic landscape: Particle filtering for indoor positioning," in *Proceedings of the European Navigation Conference*, Helsinki, Finland, May 2016.
- [36] J. Coulin, R. Guillemard, V. Gay-Bellile, C. Joly, and A. de La Fortelle, "Tightly-coupled magneto-visual-inertial fusion for long term localization in indoor environment," *IEEE Robotics and Automation Letters*, vol. 7, no. 2, pp. 952–959, 2021.
- [37] A. Canciani and J. Raquet, "Absolute positioning using the Earth's magnetic anomaly field," *NAVIGATION: Journal of the Institute of Navigation*, vol. 63, no. 2, pp. 111–126, 2016.
- [38] J. Torres-Sospedra, D. Rambla, R. Montoliu, O. Belmonte, and J. Huerta, "UJIIndoorLoc-Mag: A new database for magnetic field-based localization problems," in *Proceedings of International Conference on Indoor Positioning and Indoor Navigation (IPIN)*, Banff, AB, Canada, Oct. 2015.
- [39] R. Montoliu, J. Torres-Sospedra, and O. Belmonte, "Magnetic field based indoor positioning using the bag of words paradigm," in *Proceedings of*

International Conference on Indoor Positioning and Indoor Navigation (IPIN), Alcala de Henares, Spain, Oct. 2016.

[40] N. Lee, S. Ahn, and D. Han, "AMID: Accurate magnetic indoor localization using deep learning," *Sensors*, vol. 18, no. 5, p. 1598, 2018.

[41] L. Antsfeld and B. Chidlovskii, "Magnetic field sensing for pedestrian and robot indoor positioning," in *Proceedings of International Conference on Indoor Positioning and Indoor Navigation (IPIN)*, Lloret de Mar, Spain, Nov. 29–Dec. 2 2021.

[42] B. Siebler, S. Sand, and U. D. Hanebeck, "Bayesian Cramér-Rao lower bound for magnetic field-based localization," *IEEE Access*, vol. 10, pp. 123 080–123 093, 2022.

[43] F. M. Viset, R. Helmons, and M. Kok, "An extended Kalman filter for magnetic field SLAM using Gaussian process regression," *Sensors*, vol. 22, no. 8, 2022.

[44] I. Vallivaara, J. Haverinen, A. Kemppainen, and J. Röning, "Simultaneous localization and mapping using ambient magnetic field," in *Proceedings of IEEE International Conference on Multisensor Fusion and Integration for Intelligent Systems (MFI)*, Salt Lake City, UT, USA, September 2010, pp. 14–19.

[45] T. N. Lee and A. J. Canciani, "MagSLAM: Aerial simultaneous localization and mapping using earth's magnetic anomaly field," *Navigation*, vol. 67, no. 1, pp. 95–107, 2020.

[46] C. Gao and R. Harle, "Sequence-based magnetic loop closures for automated signal surveying," in *Proceedings of International Conference on Indoor Positioning and Indoor Navigation (IPIN)*, Banff, AB, Canada, Oct. 2015, pp. 1–12.

[47] M. Kok and A. Solin, "Online one-dimensional magnetic field SLAM with loop-closure detection," in *Proceedings of IEEE International Conference on Multisensor Fusion and Integration for Intelligent Systems (MFI)*, 2024, pp. 1–7.

[48] J. Jung, T. Oh, and H. Myung, "Magnetic field constraints and sequence-based matching for indoor pose graph SLAM," *Robotics and Autonomous Systems*, vol. 70, pp. 92–105, Aug. 2015.

[49] B. Siebler, A. Lehner, S. Sand, and U. D. Hanebeck, "Magnetic field mapping of railway lines with graph SLAM," in *Proceedings of 27th IEEE International Conference on Information Fusion (FUSION)*, Venice, Italy, Jul. 7–11 2024.

[50] S. Wang, H. Wen, R. Clark, and N. Trigoni, "Keyframe based large-scale indoor localisation using geomagnetic field and motion pattern," in *Proceedings of the IEEE/RSJ international conference on intelligent robots and systems (IROS)*, 2016, pp. 1910–1917.

[51] M. Kok, A. Solin, and T. B. Schön, "Rao-Blackwellized particle smoothing for simultaneous localization and mapping," *Data-Centric Engineering*, 2024, 5:e15.

[52] I. Vallivaara, Y. Dong, B. Duan, and T. Arslan, "Saying goodbyes to rotating your phone: Magnetometer calibration during SLAM—Extended version," *IEEE Journal of Indoor and Seamless Positioning and Navigation*, 2026.

[53] J. Li, J. Kuang, and X. Niu, "MSCEKF-MIO: Magnetic-inertial odometry based on multi-state constraint extended Kalman filter," *arXiv:2505.12634.08167*, 2025.

[54] C. I. Chesneau, M. Hillion, and C. Prieur, "Motion estimation of a rigid body with an EKF using magneto-inertial measurements," in *Proceedings of International Conference on Indoor Positioning and Indoor Navigation (IPIN)*, Alcala de Henares, Spain, Oct. 2016.

[55] M. Zmitri, H. Fourati, and C. Prieur, "Magnetic field gradient-based EKF for velocity estimation in indoor navigation," *Sensors*, vol. 20, no. 20, 2020.

[56] B. Merk, B. Siebler, and S. Sand, "Cramér-Rao lower bound for magnetic field-based velocity estimation of trains," in *Proceedings of IEEE International Conference on Multisensor Fusion and Integration for Intelligent Systems (MFI)*, College Station, TX, Sep. 2025.

[57] I. Skog, M. Nordenvaad Lundberg, E. Gudmundson, M. Brodin-Laakso, A. Gällström, A. Fagerven, and P. Sigray, "Underwater quantum magnetometer array aid inertial navigation – Feasibility and challenges: Technical report from the vinnova ENOK project 2024-03194," KTH Royal Institute of Technology, Stockholm, Sweden, Technical Report, 2025.

[58] D. Vissière, A. Martin, and N. Petit, "Using magnetic disturbances to improve IMU-based position estimation," in *Proceedings of European Control Conference*, Kos, Greece, Jul. 2007, pp. 2853–2858.

[59] S. Xu, Z. Jin, G. Jiang, G. Zhang, J. Liang, W. Sun, L. Zhang, Z. Fan, and G. Dong, "Improved towed airborne three-axis magnetic gradient anomalies navigation," *IEEE Transactions on Instrumentation and Measurement*, vol. 73, pp. 1–12, Nov. 2024.

[60] Y. Xu, Z. Liu, Q. Zhang, X. Liu, B. Huang, M. Pan, J. Hu, D. Chen, T. Ying, and X. Qiu, "Interference model guided neural network for aeromagnetic compensation," *IEEE Sensors Journal*, vol. 24, no. 8, pp. 12 266–12 275, Mar. 2024.

AUTHORS

Isaac Skog received his MSc degree in Electrical Engineering from KTH Royal Institute of Technology, Stockholm, Sweden, in 2005. In 2010, he received a PhD degree in Signal Processing from KTH Royal Institute of Technology with a thesis on low-cost navigation systems. Currently, he is an associate professor in communication systems at KTH and a senior researcher at the Swedish Defence Research Agency (FOI) in Stockholm, Sweden. He is an editor of the IEEE Journal of Indoor and Seamless Positioning and Navigation, and a board member of the Nordic Institute of Navigation. His research interest is in applied signal processing for localization and tracking. Currently, he leads multiple projects on ambient magnetic field localization.

Manon Kok received the M.Sc. degrees in applied physics and in philosophy of science, technology and society, both from the University of Twente, Enschede, the Netherlands, in 2009 and 2007, respectively, and the Ph.D. degree in automatic control from Linköping University, Sweden, in 2017. From 2009 to 2011, she was a Research Engineer with Xsens Technologies. From 2017 to 2018, she was a Postdoctoral with the Computational and Biological Learning Laboratory, University of Cambridge, U.K. She is currently an Associate Professor with the Delft Center for Systems and Control, Delft University of Technology, the Netherlands. Her research interests include probabilistic inference for signal processing and machine learning, with a specific focus on localization using inertial sensors and magnetometers.

Christophe Prieur is a senior researcher of the CNRS, at Gipsa-lab, Grenoble, France. He was the Program Chair of the 9th IFAC Symposium on Nonlinear Control Systems (NOLCOS 2013), the 14th European Control Conference (ECC 2015) and the 61st IEEE Conference on Decision and Control (CDC 2022). He has served as associate editor and senior editor of several journals, and he is currently an editor of the IMA Journal of Mathematical Control and Information. He was awarded the CNRS Silver Medal. He is an IMA Fellow and an IEEE Fellow. His current research interests include navigation, object tracking, and fluid/thermal dynamics control.

Gustaf Hendeby is an Associate Professor in Automatic Control at Linköping University, Sweden. He holds an M.Sc. in Applied Physics and Electrical Engineering (2002) and a Ph.D. in Automatic Control (2008), both from Linköping University. He has held research positions at DFKI and FOI. Dr. Hendeby is Senior Editor for the IEEE Trans. on Aerospace and Electronic Systems and Associate Editor-in-Chief of the Journal of Advances in Information Fusion. He leads the WASP Localization and Navigation Cluster and has chaired multiple IEEE FUSION conferences. He currently serves on the ISIF Board of Directors (2023–2025). His research focuses on sensor fusion and stochastic signal processing, particularly in nonlinear problems, target tracking, and SLAM.